remote sensing

MDPI

Article

A New Method to Evaluate Gold Mineralisation-Potential Mapping Using Deep Learning and an Explainable Artificial Intelligence (XAI) Model

Biswajeet Pradhan [1,2,3,*], Ratiranjan Jena [4], Debojit Talukdar [5], Manoranjan Mohanty [5], Bijay Kumar Sahu [5], Ashish Kumar Raul [5] and Khairul Nizam Abdul Maulud [3,6]

1 Centre for Advanced Modelling and Geospatial Information Systems (CAMGIS), School of Civil and Environmental Engineering, Faculty of Engineering and Information Technology, University of Technology Sydney, Sydney, NSW 2007, Australia
2 Center of Excellence for Climate Change Research, King Abdulaziz University, P.O. Box 80234, Jeddah 21589, Saudi Arabia
3 Earth Observation Centre, Institute of Climate Change, Universiti Kebangsaan Malaysia, Bangi 43600, Malaysia
4 Research Institute of Sciences and Engineering, College of Engineering, Civil Engineering, University of Shahrjah, Sharjah 2727, United Arab Emirates
5 RSAS, Geological Survey of India, Bangalore 560111, India
6 Department of Civil Engineering, Faculty of Engineering and Built Environment, Universiti Kebangsaan Malaysia, Bangi 43600, Malaysia
* Correspondence: biswajeet.pradhan@uts.edu.au

Abstract: Geoscientists have extensively used machine learning for geological mapping and exploring the mineral prospect of a province. However, the interpretation of results becomes challenging due to the complexity of machine learning models. This study uses a convolutional neural network (CNN) and Shapley additive explanation (SHAP) to estimate potential locations for gold mineralisation in Rengali Province, a tectonised mosaic of volcano-sedimentary sequences juxtaposed at the interface of the Archaean cratonic segment in the north and the Proterozoic granulite provinces of the Eastern Ghats Belt in Eastern India. The objective is to integrate multi-thematic data involving geological, geophysical, mineralogical and geochemical surveys on a 1:50 K scale with the aim of prognosticating gold mineralisation. The available data utilised during the integration include aero-geophysical (aeromagnetic and aerospectrometric), geochemical (national geochemical mapping), ground geophysical (gravity), satellite gravity, remote sensing (multispectral) and National Geomorphology and Lineament Project structural lineament maps obtained from the Geological Survey of India Database. The CNN model has an overall accuracy of 90%. The SHAP values demonstrate that the major contributing factors are, in sequential order, antimony, clay, lead, arsenic content and a magnetic anomaly in CNN modelling. Geochemical pathfinders, including geophysical factors, have high importance, followed by the shear zones in mineralisation mapping. According to the results, the central parts of the study area, including the river valley, have higher gold prospects than the surrounding areas. Gold mineralisation is possibly associated with intermediate metavolcanics along the shear zone, which is later intruded by quartz veins in the northern part of the Rengali Province. This work intends to model known occurrences with respect to multiple themes so that the results can be replicated in surrounding areas.

Keywords: gold mineralisation; modelling and mapping; CNN; XAI; GIS

Citation: Pradhan, B.; Jena, R.; Talukdar, D.; Mohanty, M.; Sahu, B.K.; Raul, A.K.; Abdul Maulud, K.N. A New Method to Evaluate Gold Mineralisation-Potential Mapping Using Deep Learning and an Explainable Artificial Intelligence (XAI) Model. *Remote Sens.* **2022**, *14*, 4486. https://doi.org/10.3390/rs14184486

Academic Editor: Thomas Cudahy

Received: 2 July 2022
Accepted: 6 September 2022
Published: 8 September 2022

1. Introduction

Generally, geological survey activities consist of mapping the composition of the crust and mineralisation by utilising both traditional and advanced methods through geochemical and geophysical techniques [1–3]. Such surveys result in integrating multisource

geospatial data that is stored as maps in a digital database. This information can be used for mineral resource identification and exploration, which is a task tailor-made for a geographic information system (GIS). The GIS is used for exploring geospatial data in a wide range and analysing layers with several geospatial models. In response to mineral-potential mapping (MPM), a GIS offers integrating approaches such as weighted overlay, logistic regression, neural networks, etc., which use controlling factors [3,4] that include geology, geomorphology, geological structure, geophysical and geochemical information to develop mineral-potential maps [5–10].

Several studies have been conducted on GIS-based mineral-potential zone estimation [10–12]. Numerous techniques were proposed, developed, and tested by many researchers to analyse mineral occurrences [11,12]. Modelling approaches recorded in the literature are data-driven approaches (in-network processing, data compression and data prediction). Statistical modelling and machine learning approaches are more subjective approaches in mineral prospectivity mapping [12]. These models depend on the expert's opinion or input information from the modeller to perform the weight calculation of conditioning factors. These methods are good for the unexplored landscapes characterised by some known deposits [13–15]. However, knowledge-driven techniques are used for any type of deposit using fuzzy logic [14,15] and the functions of the Dempster–Shafer evidence method [16–20]. Data-driven methods offer an objective approach and mostly rely on a relationship between the deposit types and the predictors. Therefore, these methods are suitable for moderate- to well-sampled areas characterised by known deposit types [21]. Several modelling methods such as the weights-of-evidence [22–25], frequency ratio (FR) [26,27], logistic regression (LR) [4,22,28] and artificial neural network (ANN) [29,30] methods were tested for mapping numerous mineral resources across different parts of the world. Surip [31] conducted a work in Penjom-Merapoh, Pahang (Malaysia) by using eight factors such as geology, faults, granite bodies, arsenic (As), tungsten (W), lead (Pb) and copper (Cu) concentrations in their research. Their study found that the Penjom Gold Mine is situated in a high-potential region with numerous favourable zones falling under a high-prospective area. In another work, McMillan et al. [32] conducted a mineral prospectivity study by developing a VNet convolutional neural network. This approach was implemented in a gold greenstone belt located in the Canadian Arctic. They implemented an algorithm for training to predict gold mineralisation deposits in the region. Xu et al. [33] conducted a study where a deep regression network was built to estimate the mineral potential in the Daqiao Gold Mine in Gansu Province, China using conditioning factors.

The current study is undertaken with the recent input of high-resolution geophysical, geochemical and geological baseline data from the Geological Survey of India to assess the prospectivity of the terrane with the aid of spatial integration. The study area has been investigated for base metal, gold and sillimanite by the Geological Survey of India (GSI) [34–36]. However, the only known base-metal prospect is from the Adash area, and gold occurrences exist near the eastern and northern parts of the study area [20,36–39]. Occurrences of gold have been reported near Sonakhani Village, Deogarh District and Odisha from the metavolcano-sedimentary assemblage of the Deogarh supracrustals lying in the northern part. The stream flowing near Jhara Gogwa of Sonakhani Village traverses the amphibolite-quartzite-minor metabasalt and quartz-sericite schist assemblage [36,37,39].

Although conventional geographical information techniques can analyse and explain multiple spatial data, the resultant models are inadequate. Moreover, in the complex geological scenario of RP, the resultant model may require highly complex processing. One of the limitations in traditional methods includes the insufficient utilisation of survey information, inaccurate model expression, and difficulty in dealing with an ample amount of geospatial data. However, no proper exposure in the RP could be found to conduct a geological or filed survey because of the inaccessible environment with complicated geotectonics [39]. However, not much work can be found on mineral-potential zone mapping using remote sensing and a geospatial dataset in the state of Odisha, India. Remote sensing data or data from the government's geological agencies were used to perform this study.

In this paper, an explainable AI-based CNN model is proposed. The recent availability of large amounts of high-resolution datasets provides a logical explanation for a realistic model, which can be achieved via this novel explainable AI (XAI) method [40,41].

Previous MPM research has focused on the quantitative extraction of anomalies, although some studies concentrated on the spatial distribution characteristics such as the coupling correlation amongst the distributions of geochemical elements, tectonics and strata outcrops using weights-of-evidence and traditional machine learning techniques [42–44]. Bonham-Carter [44] and Raines [45] conducted several studies on gold mineralisation mapping using a traditional weights-of-evidence technique that utilised a regional geoscience and GIS database. Several models, such as FR, LR, ML and deep learning (DL) models, are also used for potential zone mapping [22–28]. The database consists of geological bedrock and surficial maps, geochemical sediment samples, and airborne geophysical and mineral occurrence information. Geostructural features that include lineaments, folds and formation contacts were also considered. However, the current study includes a comprehensive assessment using detailed lithological, geophysical and mineralogical information to improve mineral-potential zone mapping using trendy and modern techniques. The relevance of different factors has rarely been considered in CNN and XAI modelling. This study has two objectives. Given that mineral occurrences are controlled by geological, geochemical and geophysical factors, the first objective is to prepare gold-potential maps by using the latest state-of-the-art artificial intelligence techniques. The second objective is to delineate possible new locales of mineral favourability areas for future mineral exploration. This work intends to identify potential favourability areas for gold mineralisation by minimising the timeline, prioritising the areas for exploration, and helping with decision-making and cost reduction.

2. Study Area

The Indian Precambrian shield comprises several "terranes" that have been amalgamated along specific boundaries [5–9]. Whilst several terrane boundaries are reportedly gradational [5], others are sharp and have been suggested to be collision zones [7]. A separate exotic, geological terrane sandwiched between the Mesoarchean Singhbhum and Bastar cratons in the north and west, respectively, and the Proterozoic orogen of the Eastern Ghats in the south has been recognised as the Rengali Province (RP). The RP is a wedge-shaped, neo-Archean terrane located in the Paleo-/Mesoarchean Singhbhum cratonic nucleus in the north between the Bastar craton in the west and Eastern Ghats Mobile Belt in the south [8,9]. The demarcation of the exact boundary between these two geological domains has not been properly resolved yet because of the intervening Gondwana sediments of the Mahanadi graben.

Geological models regarding the evolution of the terrane vary widely, considering it to be a suspect terrane [5–12], exotic/reworked terrane [5,9] or accreted arc terrane wherein granulites represent the thrusted, deep crustal section of the Singhbhum craton. The rock assemblages occupying the area between the high-grade granulites of the Eastern Ghats Mobile Belt (EGMB) and the low-grade assemblages of the cratonic granite greenstone ensemble possibly represent a distinct transitional belt. However, this terrane was designated as RP after Crowe et al. [5] and Nash et al. [9] identified not only several boundary shear zones, but also distinct lithotectonic characteristics of the terrane. The latter classified the basement rocks of RP as the Kansal and Badarama Complexes and the metavolcano-sedimentary sequences as the Pallahara complex. Crowe et al. [5] delineated a west-northwest–east-southeast (WNW–ESE) trending fault separating the Rengali and Angul lithoassemblages and marked another NW–SE trending fault along the eastern margin of the Malayagiri supracrustal belt. Lithostructurally, the central part of RP is occupied by Pal Lahara gneiss containing amphibolite and granulite patches of variable dimensions [5,46,47]. It is surrounded by low-to-medium-grade metavolcano-sedimentary supracrustal sequences, such as the Tikra, Malayagiri and Deogarh supracrustals. The Pal Lahara gneiss, along with the Malayagiri–Deogarh supracrustals, is juxtaposed against the

Singhbhum craton by an E–W trending ductile shear known as the Barkot Shear Zone [5]. The NNW–SSE trending Akul ductile fault represents the eastern boundary of RP, separating the Singhbhum craton. The NE–SW trending Riamal Shear Zone forming the Riedel pair separates the Pallahara gneiss complex from the Badrama complex. The Kerajang fault [9] broadly coincides with the north Odisha boundary fault in association with the Sukinda thrust [48]. Deformed ~1.3 Ga to 1.4 Ga alkaline nepheline syenite intrusives occur in a zone between Riamal in the west and Kamakhyanagar in the east [49–52]. A geological map of the study area is presented in Figure 1. RP hosts base-metal (mainly copper), gold and gemstone mineralisation in the Adash-Porapara-Budido-Medinipur sector [46]. Compared with the mineralisation of the Singhbhum Shear Zone [9,47], the iron ore deposits of North Odisha craton [7–12] and the chromite–PGE association of Baula-Nuasahi of this terrane has not been fully explored for its mineral potential.

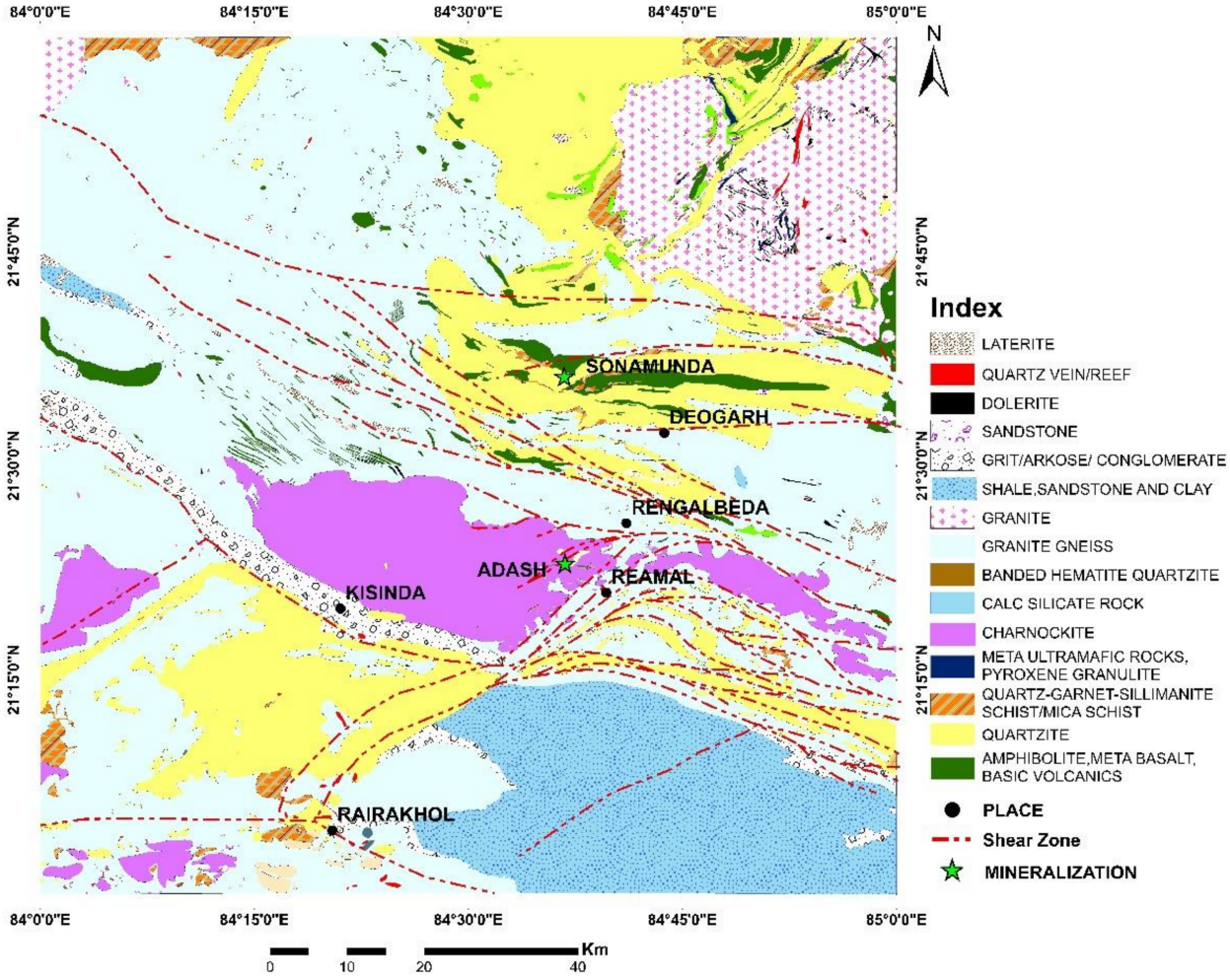

Figure 1. Study area location map.

The area has been investigated for base metal, gold and sillimanite by the Geological Survey of India (GSI) [34–36]. The only known base-metal prospect is in the Adash area (central part of the study area), and gold occurrences exist near the eastern and northern parts of the study area [36–39]. The occurrences of gossans (base-metal association) in the Budido-Medinipur-Timur and Ramapalle-Adash-Porapara areas have been investigated with the help of geophysical and geochemical methods, but no encouraging results have been obtained. In the Adash-Porapara area (west of the Adash prospect), base-metal mineralisation is confined within silicified metabasic rocks. Earlier research has shown that base-metal mineralisation is confined within high-grade metamorphics. The investigation

of base metals by the GSI near Adash has revealed the presence of malachite staining and alteration zones [37,38,40]. No multi-thematic data integration work has been carried out thus far in this study area (Figure 1). Occurrences of gold have been reported near Sonakhani Village, Deogarh District and Odisha from the metavolcano-sedimentary assemblage of the Deogarh supracrustals lying in the northern part [36,37,39]. The stream flowing near Jhara Gogwa of Sonakhani Village traverses the amphibolite-quartzite-minor metabasalt and quartz-sericite schist assemblage. The general strike of the rocks is E–W with a moderate dip toward the south. Stringers and veins of white quartz intrude into the metavolcanic, quartz-sericite schist. Panning for gold is performed during monsoons in several localities in the nearby streams. Incidences of fine gold grains have been reported whilst panning in the first-order and second-order streams around Chheliamendhia, Niktimal, Khondihi and Goilo [53,54]. Hence, the northern part of the area (covering typical locally sheared metavolcano-sedimentary rocks) appears to be a favourable target area for locating significant gold mineralisation [35].

3. Data and Methodology

Geological data, including lithological, structural and shear zone attributes, were collected from various sources [4,5,9,55,56]. All data are freely available in the BHUKOSH portal, Geological Map of India (Table 1). The study area is in the Survey of India toposheet No. 73C. The objective of the present work is to integrate multi-thematic data involving geological, geophysical, mineralogical and geochemical surveys on a 1:50 k scale with the aim to prognosticate new mineral occurrences. A lithological and shear zone map was prepared from the published data in the GSI and the available literature [5,9,56] by using in-house ArcGIS software (version 10.3). The geophysical data for gravity and magnetism were collected from the BHUKOSH portal.

Table 1. Data used for gold (Au) mineralisation-potential zone mapping.

Factors	Code Names	Sources	Resolution and Scale	References
Magnetic anomaly Bouguer anomaly	Mag_anamol Boug_anamol	Crowe et al. [5]; Nash et al. [9]; BHUKOSH portal, Geological map of India [56]	25 m and 1:50 k	The importance of all the factors mentioned are chosen based on gold group elements (gold, silver, copper, mercury, aluminium and lead) [55,57,58]
Antimony (Sb) Lead (Pb) Arsenic (As) Aluminium (Al) Mercury (Hg) Tin (Sn) Cobalt (Co) Cupper (Cu) Quartz (SiO_2)	Sb_con Pb_con As_con Al_con Hg_con Sn_con Co_con Cu_con SIO_2_con			
Lithological map Shear zone Lineament map	Lith_gold Dist_shear Linea_den			
OLI-Landsat 8 (silica) OLI-Landsat 8 (clay)	Oli_silica Oli_clay	United States Geological Survey (USGS)		

The raw geophysical data collected at a station interval of 2.5 km^2 were processed following standard published protocols by using in-house Geosoft software. The geochemistry of soil samples from every 1 km^2 (sample from every 1 km^2 area) from the first-order stream was analysed by the GSI under the aegis of the National Geochemical Mapping Programme (NGCM) and made available in the BHUKOSH portal. The soil samples were analysed for a set of 64 elements by following international protocols and several national/internal standards. The geochemical maps were created using inverse distance weighting (IDW) interpolation of the values of geochemical elements. For the geochemical and geophysical

data, certain parts of the study area are devoid of any value due to the forest/sanctuary cover [57]. Landsat-8 (OLI) is a multispectral, nine-band land imager whose data type can be downloaded from the United States Geological Survey website. Out of the nine bands, seven are consistent with the Thematic Mapper and Enhanced Thematic Mapper Plus (ETM+) sensors found in earlier Landsat satellites and are thus compatible with historical Landsat data. Bands 1 to 9 have a spatial resolution of 30 m, whereas band 8 (panchromatic) has a spatial resolution of 15 m. The required amount of noise-free data was obtained for the study, and after corrections and image processing, band-ratio maps were prepared in ERDAS Imagine-14 software. Lineament maps were prepared based on the National Geomorphology and Lineament Project database (Geological Survey of India) and extracted from remote sensing (Landsat-8 OLI and Advanced Spaceborne Thermal Emission and Reflection Radiometer (ASTER)) data [58].

3.1. Detailed Description of Factors

Mineral prospectivity mapping (MPM) is a multifactorial modelling activity. It is a futuristic framework for potential zone identification that involves geoscientific data from multiple sources, such as geochemical, mineralogical, geophysical and geological surveys (Figure 2). The details of these factors are provided [59–61].

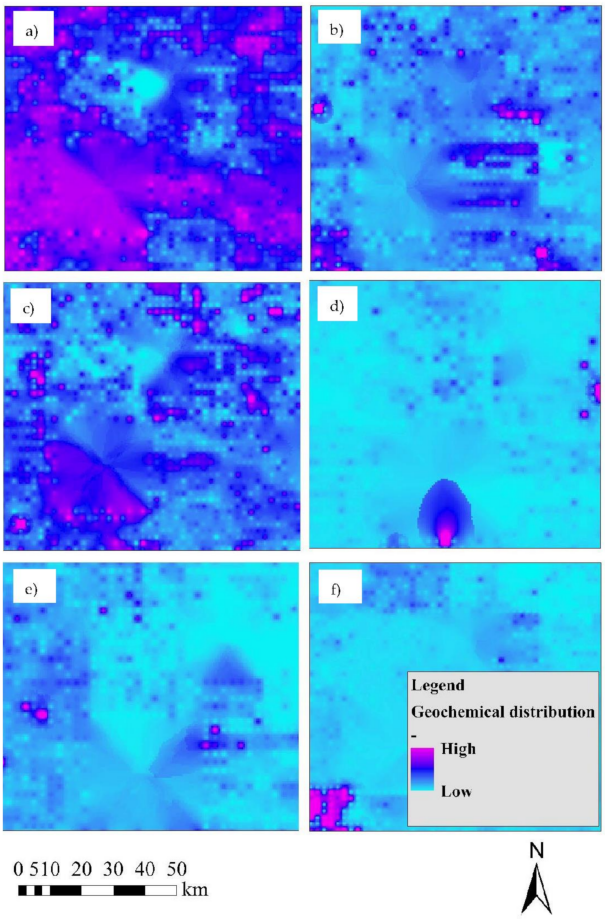

Figure 2. *Cont.*

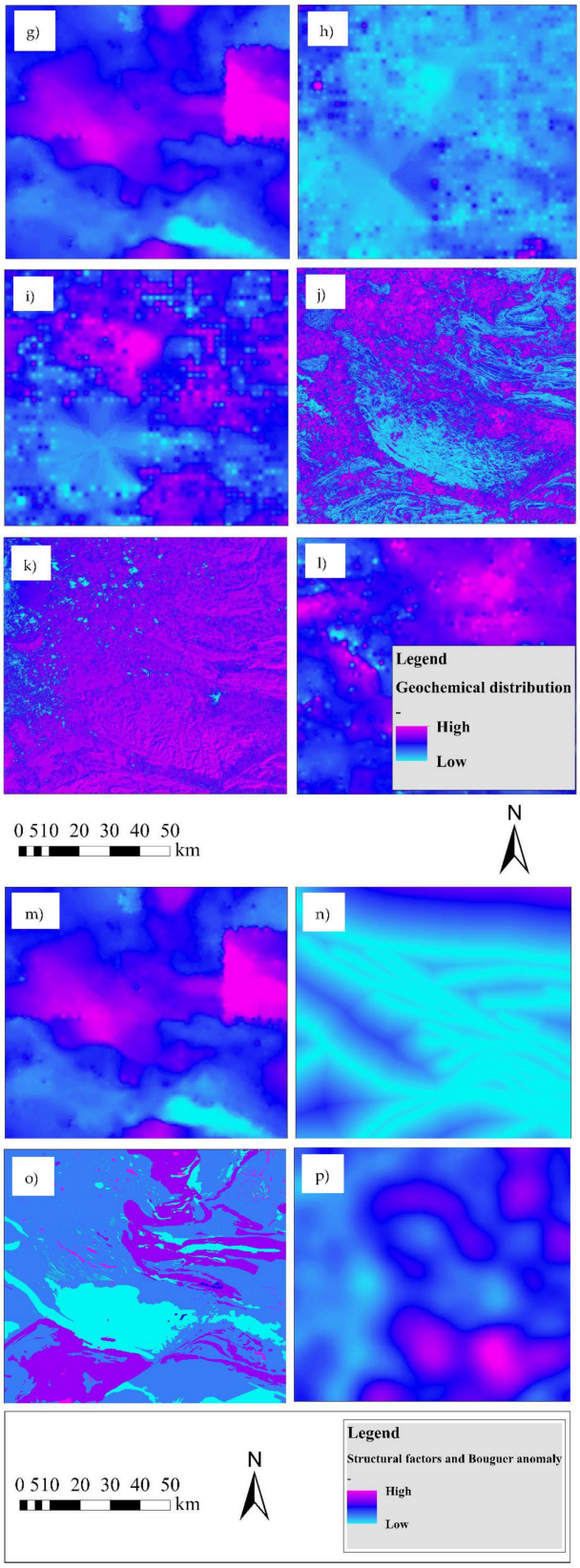

Figure 2. Factors considered in CNN and XAI models for gold (Au) mineralisation-potential zone mapping. (**a**) Al_con, (**b**) Sb_con, (**c**) Co_con, (**d**) Sn_con, (**e**) Hg_con, (**f**) As_con (continued), (**g**) Cu_con, (**h**) Pb_con, (**i**) SiO_2_con, (**j**) Oli_silica, (**k**) Oli_clay, (**l**) Mag_anamol (continued), (**m**) Boug_anamol, (**n**) Dist_shear, (**o**) Lith_gold, and (**p**) Linea_den.

3.1.1. Geochemical Factors

Geochemical anomalies were considered for gold-potential zone mapping. The element contents of antimony (Sb), lead (Pb), arsenic (As), aluminium (Al), mercury (Hg), tin (Sn), cobalt (Co), copper (Cu) and silica (SiO_2) in the samples were used as the indicators/pathfinders for gold occurrences. These elements are sometimes found in association with gold. The point data of each element concentration were converted into raster maps via the IDW interpolation algorithm. A pixel size of 444 m × 444 m was used to generate prospectivity maps in this study. These interpolated maps were utilised in a convolutional neural network (CNN) model to predict the binary targets. Similarly, all other predictive factors (geophysical, geological and mineralogical) were generated using the GIS platform for gold-potential zone mapping. The gold values from the first-order stream sediment sample ranged from 1.5 ppb to 348 ppb. The northern and northeastern parts in the north of Deogarh Town, Odisha, show anomalous gold values [37,39]. The rock types are metavolcanic sedimentary lithopackages in association with granite [54].

3.1.2. Geophysical Factors

Geophysical investigations provide an alternative approach for the prediction and potential mapping of mineralised zones, where limited baseline data are available and a highly complex geotectonic environment exists [62,63]. The use of traditional geophysical techniques reveals subsurface continuity along with the detailing of deposits in mineral exploration. This approach provides results that enable cost reduction and can replace borehole techniques [64,65]. Studies have supported the usage of geophysical information in the exploration of gold occurrences [66,67].

3.1.3. Geological/Structural Factors

Although gold occurrences have been reported in the northern part of the study area (near Sonakhani Village, Deogarh District, Odisha) from the metavolcanic sedimentary assemblage of Deogarh supracrustals [36,37,39], fine-grained gold is mostly documented from the extensive panning. The amphibolite sequence is interlayered with quartzite, which forms ridges and amphibolite peneplains. The alteration is prominent, and this Archaean metasedimentary package may serve as an ideal package for gold occurrences. The stream drains near Jhara Gogwa of Sonakhani Village, north of Deogarh District in Odisha, and traverses the typical, sheared amphibolite-quartzite-minor metabasalt and quartz-sericite schist assemblage. Incidences have also been reported from the first-order and second-order streams around Chheliamendhia, Niktimal, Khondihi and Goilo [54]. Hence, the northern part of the area with the typical, sheared lithoassemblage is an obvious target area for locating significant gold mineralisation [35]. Low-to-medium-grade (dominantly in amphibolite-grade) metavolcano-sedimentary rocks can therefore be of significance; moreover, secondary placer gold accumulations in colluvial/alluvial deposits have been revealed in this province [35]. In addition, the sheared lithological assemblage and the proximity of shear zones act as a major controlling factor for such occurrences [39]. Shear, which developed later than the last phase of folding in the Adash base-metal prospect, might have helped in dissipating copper mineralisation [34]. This condition implies that regional shear may possess control over mineralisation [39]. Therefore, all these factors were considered for the gold-potential mapping in this study.

3.1.4. Mineralogical Factors

Several types of remote sensing data, such as data from Landsat-8, Landsat Enhanced Thematic Mapper+ (Landsat-7 ETM+) and ASTER, have been used by several researchers to detect and map hydrothermal mineralisation [68,69]. These data help detect epithermal gold mineralisation in quartz-bearing veins. Clay and quartz can also serve as a pathfinder for gold mineralisation. Landsat-8 data such as the OLI remote sensing data were collected and used to identify hydrothermal alteration zones associated with the clay and silica deposits. The FLAASH algorithm was implemented for preprocessing and the DPCA method

was adopted for alteration zone mapping. Then, this information was used as thematic layers for the gold mineralisation mapping. Near Telikusum Village (in the northern part of the study area), hard, massive amphibolite has been found to be altered and exhibits chloritisation and ferruginisation [39]. The alteration is prominent, and this Archaean metasedimentary package may serve as an ideal package for gold occurrences. Therefore, these pieces of information (i.e., Oli_clay and Oli_silica data) were also included in this study as two predictive factors for gold-potential zone mapping.

3.2. CNN

A CNN is a specialised network that integrates the invariance information of 2D shapes by imposing restrictions on the weights between neurons and using connection patterns [70]. The convolutions are the distinguishing component for feature extraction in a CNN model. The convolution of a filter $f(x, y)$ and a data function $g(x, y)$ can be expressed as:

$$c(x,y) = \sum_{t=-\infty}^{\infty} \sum_{s=-\infty}^{\infty} f(s,t) \times g(x-s, y-t) \quad (1)$$

where $c(x, y)$ denotes the convolution product, and t and s are the position parameters. Figure 3 demonstrates the procedures of CNN convolution. The filter function $f(x, y)$ is also known as a convolutional kernel. The CNN's capabilities depend largely on convolutional filters [71]. The amalgamation of activation functions, the loss function and backpropagation help in training convolution filters and weights for fully connected layers. For improved performance, max-pooling and activation functions that add nonlinearity can be applied to reduce the dimensionality and assist in solving nonlinear problems. The loss function is used to estimate the interval between the results obtained by the model and the ground truth. In this study, the *softmax* cross-entropy function was selected as the activation and loss function. The results of the CNN are a set of values. The *softmax* function converts these numbers into probabilities between 0 and 1 as follows:

$$Softmax(y_i) = \frac{e^{y_i}}{\sum_{i=1}^{n} e^{y_i}} \quad (2)$$

where n denotes dimensionality and y_i denotes the model output. Generally, the cross-entropy function estimates the distance between the labels (1 and 0 for gold and non-gold classification, respectively) and probability distribution. The cross-entropy function, $H(p, q)$, can be expressed as:

$$(p,q) = -\sum_{x} p(x)\, logq(x) \quad (3)$$

where $p(x)$ denotes the distribution of labels and $q(x)$ is the probability distribution. The Adam optimiser was used in this study to reduce the distance between the CNN output and the ground truth [72]. The Adam optimiser estimates proper learning rates by updating weights and using loss function gradients. This adjustment process is known as backpropagation. When all the weights have been learned using the backpropagation algorithm, the CNN model can be used for classification and prediction purposes.

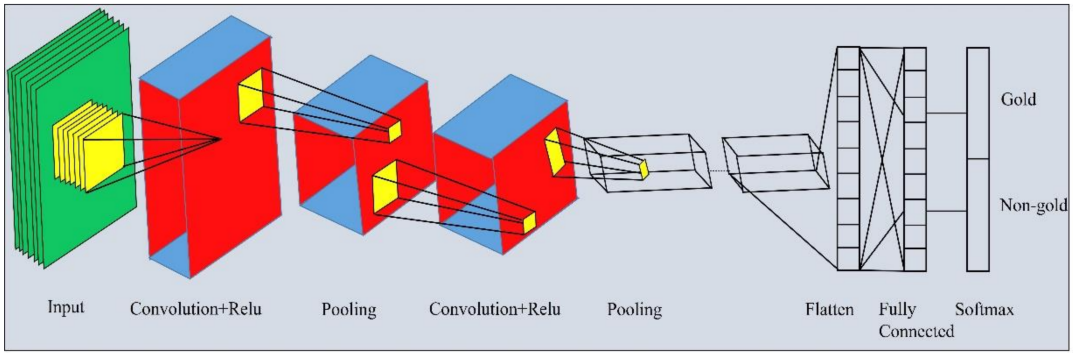

Figure 3. Architecture of CNN model for gold mineralisation mapping.

3.3. XAI Model

The XAI (i.e., Shapley additive explanation or SHAP) has been applied to CNN models to create additive attributes that help identify significant factors and determine the effects on model outputs. The SHAP technique adopts the concept of game theory, and it allocates an importance value to each factor on the basis of the impact on prediction. The existence of factors is considered in the SHAP estimation [73]. A linear additive feature attribute method is utilised in the SHAP to explain complex AI models as follows:

$$f(a) = g(a') = \varnothing_0 + \sum_{j=1}^{J} \varnothing_j a'_j \quad (4)$$

For an original method $f(a)$, the explanation model $g(a')$ and J are the mineralisation mapping attributes, $\varnothing_0$ is the output without any attributes, $\varnothing_j$ denotes the SHAP values and input vector a'_j indicates the occupancy of a specific attribute. Therefore, the SHAP can describe local and global models.

3.4. CNN Architecture and Implementation

Comprehensive geochemical data on gold were collected from the study location. The spatial resolution of the individual database was identical (i.e., 1:50 k), which is apt enough to provide a detailed view of the result over the study area. The resolution was chosen because the acquired data resolution at the start was 1:50 k. Then, several non-gold points were randomly generated using ArcGIS 10.6 to train the CNN model. The input data were prepared at data points for 16 layers. In a random subset, 80% of the spectrograms were selected as a training set (Figure 3). Next, a CNN model was developed for gold-potential zone mapping that continuously scanned through 16 indicators and convolutional layers and classified gold and non-gold locations (Figure 4). The CNN model was applied in TensorFlow (version 2.6, Google Inc., USA) and Python 3.5. The CNN architecture is composed of six layers, including the input and output layers. The CNN hyperparameters were experimentally explored for performance optimisation. This study applied the binary classification technique to evaluate the model's performance. The trained dataset comprised 1403 samples, where 903 samples were positive (gold) and 500 samples were negative (non-gold). Out of the 1403 data points, 1122 and 281 samples were used for training and validation purposes, respectively.

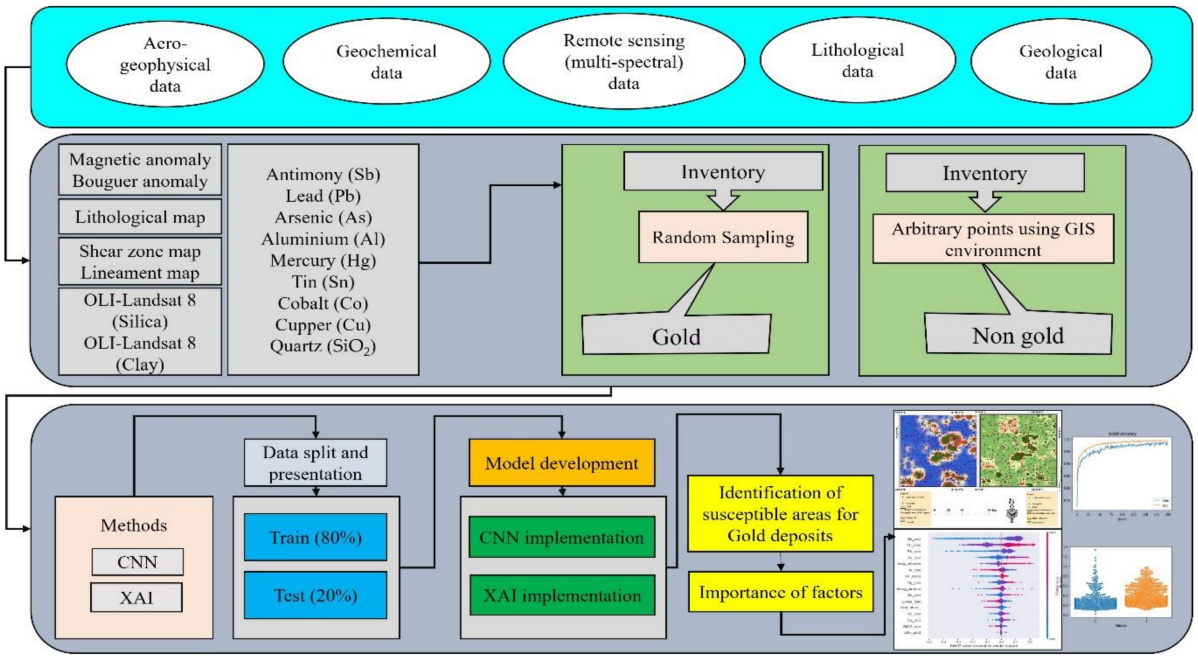

Figure 4. Methodological flow chart for gold (Au) mineralisation-potential zone mapping.

A dataset for the entire study area was created (1 million points) for testing to estimate the values for each point and was used later on for probability/favourability mapping. With regard to optimisation, the Adam optimiser was implemented to optimise the model, and batch size (32), validation split (0.2) and verbose (1) were applied to avoid overfitting epochs (200). The CNN model was trained with a total of 124,402 trainable parameters (Table 2). The classifier predicted the targets as 0 and 1 with an accuracy of 90%. In the next step, postprocessing was conducted to convert the pixels to raster images to generate the potential map.

Table 2. Trainable and non-trainable parameters for the CNN model.

Layer (Type)	Output Shape	No. of Parameters
dense_1 (dense)	(None, 200)	3400
dropout_1 (dropout)	(None, 200)	0
dense_2 (dense)	(None, 200)	40200
dropout_2 (dropout)	(None, 200)	0
dense_3 (dense)	(None, 200)	40200
dropout_3 (dropout)	(None, 200)	0
dense_4 (dense)	(None, 200)	40200
dropout_4 (dropout)	(None, 200)	0
dense_5 (dense)	(None, 2)	402
Total parameters: 124,402		
Trainable parameters: 124,402		
Non-trainable parameters: 0		

3.5. Learning the Model Parameters and Performance

The CNN was trained for one epoch on this dataset before the final supervised training of 32 epochs. The weight of the data layers was updated in the distant and supervised training phases through backpropagation.

Accuracy is a simple measure of a classifier's performance [74,75].

$$Accuracy\ (ACC) = \frac{Number\ of\ correctly\ labeled\ samples}{Number\ of\ all\ testing\ samples} \tag{5}$$

Precision is the representation of the measure of quality, and recall demonstrates the measure of quantity.

$$Precision = \frac{TP}{TP + FP} = 1 - FPR \tag{6}$$

$$Recall = \frac{TP}{TP + FN} \tag{7}$$

The accuracy (ACC), false positive rate (FPR), true negative rate (TNR), true positive (TP), true negative (TN), false positive (FP) and false negative (FN) are mentioned in the equations.

The F1 score is computed from precision and recall (i.e., the harmonic mean) of each class.

$$F1 = \left(\frac{precision^{-1} + recall^{-1}}{2} \right)^{-1} \tag{8}$$

4. Results

A heat map was generated using all 16 factors for correlation (Figure 5). This map provides a visual summary of data and helps in perceiving complex information [76]. A numeric value can be obtained for each cell, and all values varying between −1 and 1 can be reported in a standard data table. Values ranging from small to large are denoted by colours ranging from light to dark, respectively. In simple terms, this map shows the relationship between attributes and signifies the impact of certain attributes on others. It

presents a pairwise comparison of factors where the diagonal values are 1, as presented in Figure 4. Positive, negative and no effects can be observed in the attributes. In supervised learning, attributes that are important are generally considered in determining the target that can be generated based on the heat map results. The heat map shows that geochemical factors have more importance than geological factors.

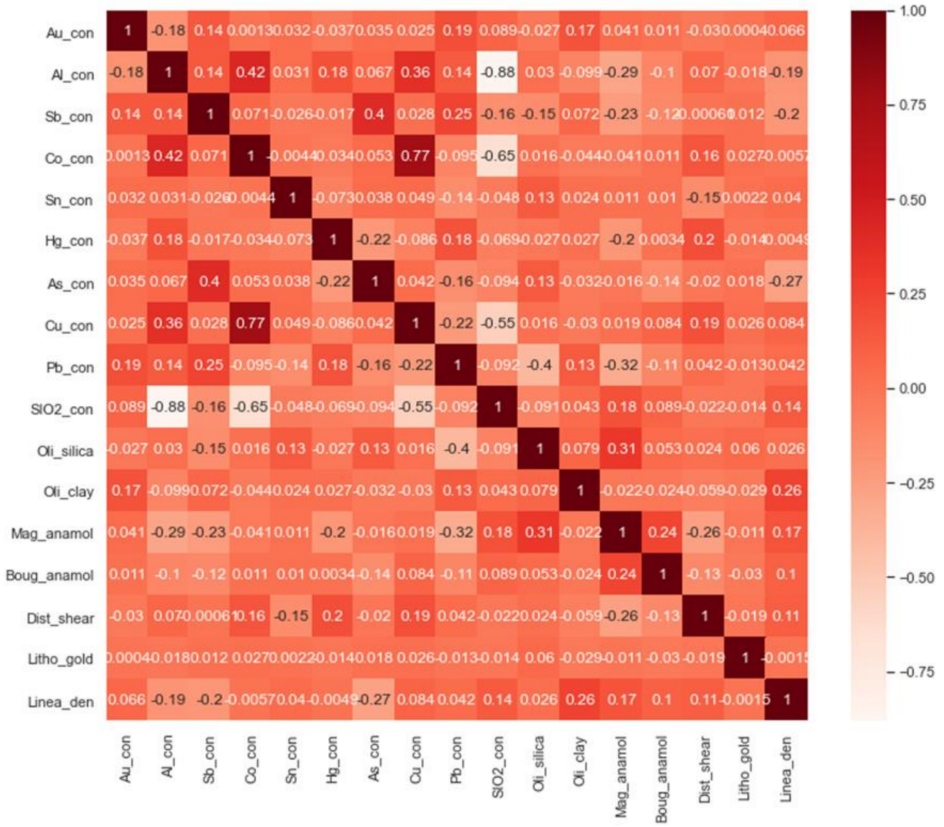

Figure 5. Heat map presents the correlative relationship among factors.

The idea behind the SHAP feature importance estimation is to understand the impact of factors on the model output. The SHAP interpretation reveals the factors with a high importance, and large, absolute Shapley values can contribute to the CNN model for gold-potential zone mapping. In this study, the average impact of each factor was estimated with respect to impact magnitude. According to the results, Sb_con (0.16 ppm), Oli_clay (0.12 ppm), Pb_con (0.06 ppm), As_con (0.05 ppm) and Mag_anamol (0.04 ppm) have high impacts (Figure 6a,b). To estimate the global importance, this study summed up all the absolute Shapley values for a particular factor across the data. In general, SHAP feature importance is based on the magnitude of factor attributions, whereas permutation feature importance depends on model performance. The feature importance plot only contains importance, which is not informative.

Therefore, a summary plot that combines feature importance with feature effects was plotted. The summary plot shows the Shapley value for each point on a factor and an instance. The y-axis represents the position, and the x-axis shows the Shapley value. The factor values are presented in colours ranging from low to high. Overlapping points are shown as jittered on the y-axis to help understand the nature of the distribution of the Shapley values. The features are ordered in the graph on the basis of their importance (Figure 6b).

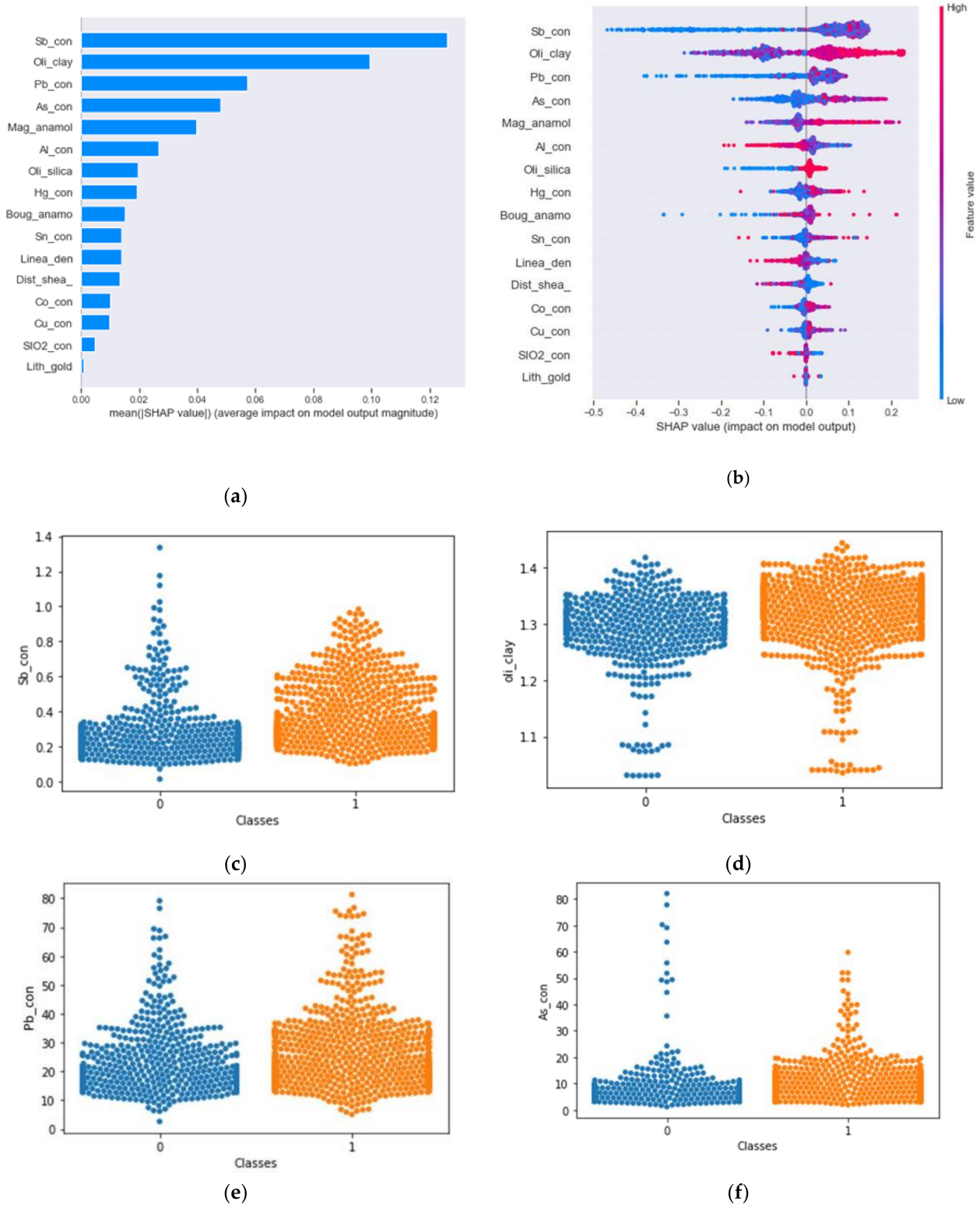

Figure 6. (**a**) Importance of factors based on SHAP values, (**b**) summary plot based on SHAP values for all factors for potential zone mapping, (**c**) swarm plot showing the distribution of highly significant attributes (Sb_con) for the gold and non-gold classes, (**d**) Oli_clay, (**e**) Pb_con and (**f**) As_con.

According to the results, the impact of the values on the model output for each data point varied; examples include Sb_con (−0.5–0.2), Oli_clay (−0.3–0.25), Pb_con (−0.4–0.1), As_con (−0.2–0.2) and Mag_anamol (−0.1–0.2) (Figure 6a,b). Swarm plots were plotted for

the highly significant factors, such as Sb_con, Oli_clay, Pb_con and As_con for gold and non-gold classes, as presented in Figure 6c–f. The significant factors varied with respect to the two classes. More gold classes were found than non-gold classes in the Sb_con anomaly range of 0.1–0.5 ppm. More gold classes can be found in the Oli_clay range of 1.2 to 1.4 ppm than non-gold classes. Similarly, more gold classes were found in Pb_con (10–40 ppm) and As_con (1–20 ppm) than in non-gold classes. Therefore, these factors are significant for predicting gold locations. The geochemical targets and the known gold occurrences were under the high-potential zones. The training and testing accuracies obtained by the CNN model reached 96% and 90%, respectively. The estimated loss from this model was compared across the epochs. The obtained baseline error was 9.25%, and the final accuracy was 90% (Figure 7).

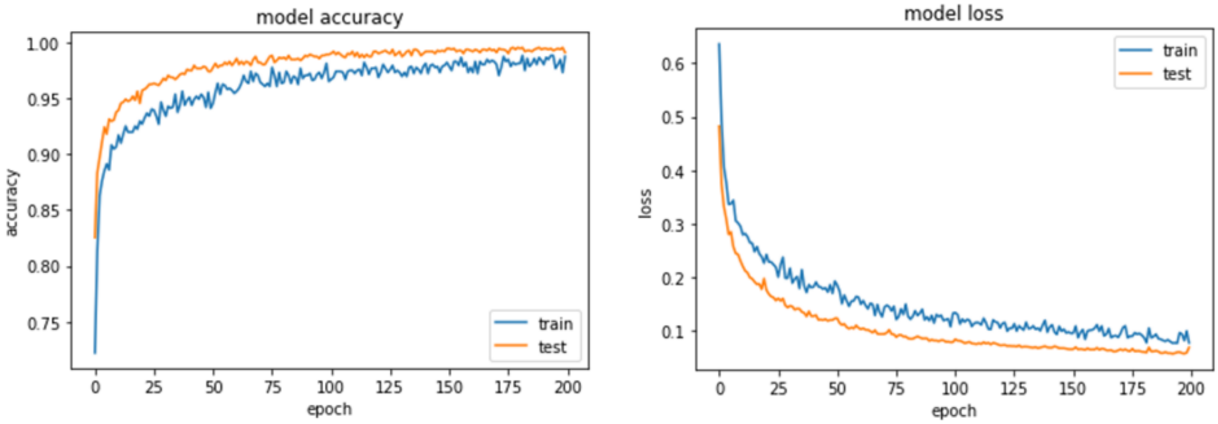

Figure 7. (**a**) Accuracy and (**b**) loss estimation for the CNN model.

The confusion matrix (Table 3) and classification report show the details about macro- and weight averages, respectively. No pattern was observed in FNs in the confusion matrix. The precision, recall, F1 score and support for the non-gold (0) class were 0.92, 0.81, 0.86 and 100, respectively; the values for the gold (1) class were 0.90, 0.96, 0.93 and 181, respectively. The TP (81), FP (7), TN (174) and FN (19) values were obtained based on the confusion matrix.

Table 3. Confusion matrix obtained from CNN model prediction.

		Predicted	
Actual		**Positive**	**Negative**
	Positive	81	19
	Negative	7	174

Training was conducted with the augmented data on 16 major factors, including geochemical, remote sensing and geophysical data, in the training area. The CNN model performed well in locating favourable locations for gold mineralisation through the spatial maps of RP, India. The prospectivity output of the CNN model showed the high- (410) and low-prospectivity areas (0) and exhibited a good spatial correlation with known mineralisation based on the geochemical study. Sb, Pb, As, Al and Si, including clay, were located in the high-probability areas of gold. According to the results, all high-probability areas in the central, southern and SW parts of the study area were characterised by known occurrences.

This result indicates that anomalous elemental values occur along with gold in the high-probability locations on the map and serve as an indicator for mineralisation mapping. As previously mentioned, this study was conducted to estimate the spatial probability of

base metals, gold and sillimanite. Gold occurrences were reported near Sonakhani Village, Deogarh District, Odisha by GSI. Another map was generated by conducting a geochemical analysis to check the probable locations with gold values varying between low (0.015 ppb) and high (409.22 ppb). The obtained map based on geochemical analysis showed similar potential locations as the map generated by the CNN model. The high-probability areas are also in the NE part of the study area. The central part of the area is large, implying a high potential for containing undiscovered occurrences because of the mineral-rich shear zone. The gold prospective map demonstrates that the shear zone is also a suitable location for gold occurrences. Gold occurrences in RP could be the epithermal type, which is generally associated with the sheared, interlayered, metavolcano-sedimentary sequence, and may be similar to that of Singhbhum Province [77,78] in terms of the source and regional geology [5,37,54]. These results suggest that a CNN with augmented data is useful for MPM and feasible for use in further explorations. Approximately 5–7% of the province is expected to be characterised by gold occurrences according to the obtained results (Figure 8).

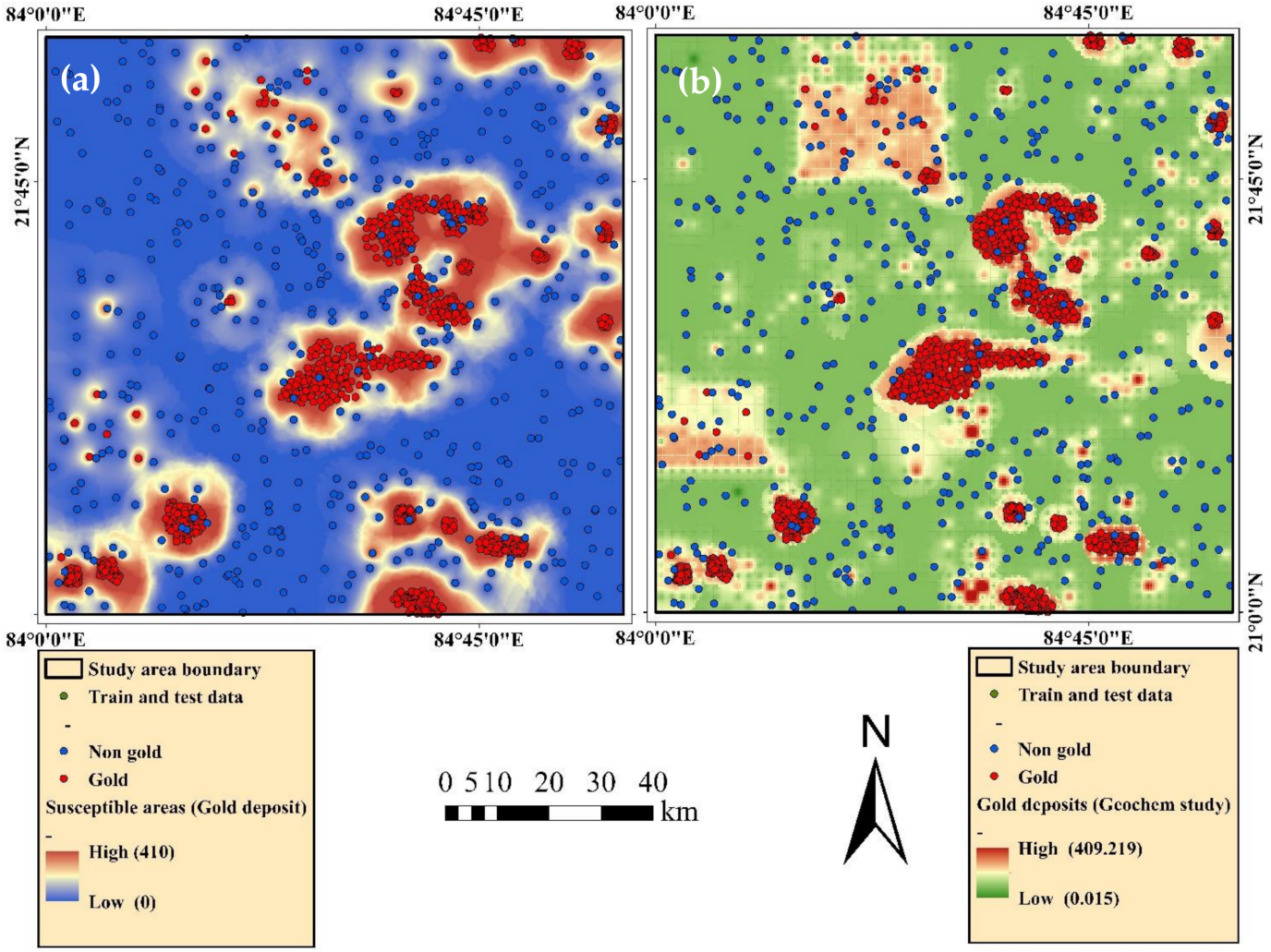

Figure 8. (**a**) Mineralisation-potential zone for gold based on CNN model, and (**b**) geochemical study-based gold bearing locations.

5. Discussion

The Shapley approximation was implemented to estimate the importance of predictive factors for gold-potential zone mapping. On the basis of relative importance, individual factors were utilised in the CNN predictive model to map gold-potential zones. The Sb_con anomaly was the most significant factor, followed by As_con, Pb_con and Oli_clay. The

Sb_con anomaly can thus be considered the direct pathfinder for targeted gold mineralisation. In RP, specks of gold have been found to be great dispersed in the stream environment, and fine-grained gold has been mostly documented from extensive panning. The streams traversing the interlayered amphibolite-quartzite sequence are significant. Therefore, a geochemical analysis of stream sediments could be the most useful tool for gold exploration and is still a primary technique for ground surveying and research [79]. The geochemical Au_con anomaly is considered a target for gold-potential zone mapping because gold is its own best geochemical pathfinder [79]. Therefore, high Au concentration values can be found over metabasalts, amphibolites and basic volcanics above 13.80 ppb, and the highest concentration is 410 ppb with the standard deviation of 47.96 ppb (Table 4). The Sb content varies from 0.01 to 1.34, and an average of 0.34 ppm was found in the study location, whereas the standard deviation was 0.18 ppm. Given that the Sb_con average was more than the average continental crust value, it is another pathfinder for gold. Oli_clay is the second important pathfinder for gold, with values ranging from 0 ppm to 1.6 ppm. The Pb_con anomaly varies from 2.63 ppm to 81.29 ppm, and the average value is 24.96 ppm; it is also an individual pathfinder for gold with a standard deviation of 11.85 ppm. In RP, the mercury (Hg) values range from 0.1 ppb to 369.6 ppb, and an average of 12.89 ppb can be observed.

Table 4. Basic statistics of the major elemental concentrations in the study area.

Major Concentrations	Minimum	Maximum	Sum	Mean	Standard Deviation
Au_con (ppb)	1.42	410	48743.52	34.72	47.96
Sb_con (ppm)	0.015	1.34	475.45	0.34	0.18
Pb_con (ppm)	2.63	81.29	35039.13	24.96	11.85
As_con (ppm)	1.13	82.08	12491.84	8.90	7.79

Fifty percent of the values exceed the average value of 56 ppb in the upper continental crust. Generally, high concentrations of Hg with values of more than 15.14 ppb (α for Hg) can be found in metabasalts and conglomerates. The As concentration value ranges from 1.13 ppm to 82.08 ppm with an average of 8.90 ppm and standard deviation of 7.79. Ninety percent of the samples have As values above 1.5 ppm of the average value of the upper continental crust, according to Behera et al. [42].

Gold occurrences are mostly found as greenstone-hosted, lode and sediment-hosted gold deposits or as Archaean quartz-pebble conglomerate placers [77,78,80–83]. In the Indian subcontinent, gold metallogeny is episodic from the Mesoarchean to Neoproterozoic periods, peaking in the Neoarchean and Paleoproterozoic periods [83]. The gold deposits are commonly a lode type or vein/reef type restricted to shear zones. Secondary shear zones or splays act as the loci for mineralisation; deformed/metamorphosed host rocks in association with sulphides exhibit extensive wall rock alterations along the mineralised zones [78,83]. The main sources of gold occurrences could be the interlayered sheared amphibolite-quartzite sequences in association with quartz veins in RP. The occurrences are mostly found in the streams traversing the abovementioned sequences. Panning for gold is performed during monsoons in several localities in the nearby streams [5,36,37,54]. A nearly similar situation is observed in Singhbhum Province, where the gold in the cratonic core region occurs either as greenstone-hosted lode gold or as a modified paleoplacer, whereas in the North Singhbhum Mobile Belt it is associated with quartz reefs and auriferous sulfides hosted by greenschist-amphibolite facies rocks [78]. Hydrothermal fluids derived from concealed granitic batholiths could be another source for gold mineralisation [84]. Behera et al. [42] stated that during the Early–Middle Triassic, multiple gold-polymetallic mineralisation events in association with felsic magmatism occurred in the adjacent Sonakhani Greenstone Belt. Hence, the available geological clues have been integrated whilst carrying out the study.

Behera et al. [42] integrated the fuzzy analytical hierarchy process (FAHP) with the concentration-area (C-A) fractal model by using the GIS platform for gold-potential zone

mapping in the Sonakhani Greenstone Belt, India. This study regarded the pathfinder elements (Au, As, Ag, Hg, Sb and Se) as predictive factors (independent variables). This study validated that already identified gold-enriched blocks can be adopted for the successful prediction of potential zones. This study area was subjected to a multifractal approach based on follow-up activity, which validated the CNN results. Zhang et al. [43] applied three approaches, namely, the support vector machine (SVM), backpropagation (BP) neural network and weights-of-evidence (WOE) method, to map potential zones for gold in the Hatu region of Xinjiang in northwestern China. The area under the curve (AUC) for the SVM, BP and WOE methods was 0.811, 0.825 and 0.790, respectively. Their results showed that high accuracy can be achieved by BP when the AUC ranges within 0.7–0.9. In a recent work, Zhang et al. [85] conducted MPM by using a data-driven method known as an unsupervised convolutional auto-encoder network (CAE)-based CNN for geoinformation synthesis. Sun et al. (2020) used a set of machine learning models, such as the SVM, random forest (RF), ANN and CNN models, for tungsten (W) prospectivity mapping in Jiangxi Province, China. The study recorded an overall accuracy of 95%. The highest accuracy in correctly classifying samples was recorded by the CNN model with 92.38%, followed by the SVM (85.71%) and RF (87.62%) models; the ANN (85.24%) had the lowest accuracy. The current accuracy based on the CNN shows that the model is suitable for gold mineralisation mapping (Table 5).

Table 5. Classification report of the CNN model.

	Precision	Recall	F1-Score	Support
Non-gold	0.92	0.81	0.86	100
Gold	0.90	0.96	0.93	181
Accuracy			0.91	281
Macro-average	0.91	0.89	0.90	281
Weighted average	0.91	0.91	0.91	281
Classification accuracy: 0.90				

Gold mineralisation is a rare phenomenon. Ground truth and known occurrences are scarce compared with non-mineralised locations, thus making the CNN fail to relate predictive (all factors) and target (random and known mineral locations) variables accurately [85]. Furthermore, uncertainty in mapping potential mineralisation could arise because the target variable varies from a mineralisation trace to typical deposits. According to the results, the CNN model has an accuracy rate of 90% and a higher capability in mapping gold-potential occurrences compared with traditional machine learning algorithms.

6. Conclusions

This study used a CNN model for native gold-potential zone mapping. Geochemical data with a small number of known mineral (economic point of view) occurrences as well as geophysical, geological and mineralogical data were utilised to build and train a CNN model. The mapped areas exhibited a strong spatial correlation with the known mineral occurrences, and most of the known mineral occurrences were located in high-probability areas in the developed gold-potential map. The obtained results proved the adequacy of the CNN model for integrating multisource geoscience data and its feasibility for guiding further explorations. This study also created a mineral-potential map for RP that highlights the gold prospective zones. The central, northeastern, south and southwestern parts of the province were considered high-potential zones for gold mineralisation. All potential locations had undiscovered gold mineralisation due to the favourable sheared interlayered metavolcano-sedimentary sequences. The potential zones were verified through geochemical analysis and known gold occurrences.

Recognised pathfinders are not always meticulous factors and disregarding the ones that are deemed irrelevant for mineral-potential zone mapping is not good. Therefore, a set of quantitative prediction models must be established to simultaneously create a

geological background and big data for prediction. Accordingly, the prediction models of big data and the AlexNet algorithm of the D-CNN, which has been proven effective in depicting complicated and nonlinear spatial predictions, could be adopted in future research. This study proposed a SHAP model that can reveal the relevance of various factors for gold-potential mapping.

The proposed CNN model is effective in gold-potential zone mapping by synthesising multi-geoinformation. The next investigative step for predictive work in the study area will focus on high-favourability metallogenic locations in RP that are not known to contain occurrences. For the detailing of mineral-potential occurrences, a stream-based grid sediment sampling analysis, thematic mapping characterisation of volcano-sedimentary lithopackages and local pitting–trenching followed by suitable ground geophysical techniques can be used in the future. The CNN model used in the current work provides insights into the adoption of data-driven methodologies for gold-potential mapping in similar environments. The produced maps could be enhanced further by using highly developed AI methods, including local interpretable model-agnostic explanations and class activation mapping, and more geochemical, structural, geological, geophysical and satellite data.

Author Contributions: Conceptualisation, B.P.; methodology, B.P. and R.J.; software, B.P.; validation, D.T., M.M., B.K.S. and A.K.R.; formal analysis, D.T., M.M., B.K.S., A.K.R., R.J. and B.P.; investigation, D.T., M.M., B.K.S., A.K.R., R.J. and B.P.; resources, B.P., D.T., M.M., B.K.S. and A.K.R.; data curation, D.T., M.M., B.K.S., A.K.R., R.J. and B.P.; writing—original draft, B.P., R.J., D.T., M.M., B.K.S., A.K.R., R.J. and K.N.A.M.; writing—review and editing, B.P., R.J., D.T., M.M., B.K.S., A.K.R., R.J. and K.N.A.M.; visualisation, B.P., R.J., D.T., M.M., B.K.S., A.K.R. and K.N.A.M.; supervision, B.P.; project administration, B.P., D.T., M.M., B.K.S. and A.K.R.; funding acquisition, B.P. All authors have read and agreed to the published version of the manuscript.

Funding: The study is supported by the Centre for Advanced Modelling and Geospatial Information Systems (CAMGIS), University of Technology Sydney. Also, partly supported by the UKM YSD Chair of Sustainability (UKM-YSD-2021-003).

Data Availability Statement: Most of the data was collected by the Geological Survey of India. The publicly archived datasets used for the analysis are cited in the manuscript. The GIS analysis and machine learning part was carried out at University of Technology Sydney, and the derived data can be provided upon request to the author (biswajeet.pradhan@uts.edu.au).

Conflicts of Interest: The authors declare no conflict of interest. The funders had no role in the design of the study; in the collection, analyses, or interpretation of data; in the writing of the manuscript; or in the decision to publish the results.

References

1. Naqvi, S.M.; Naqvi, R.; Rogers, J.J.W. *Precambrian Geology of India*; Oxford University Press: New York, NY, USA, 1987.
2. Knox-Robinson, C.M. Vectorial fuzzy logic: A novel technique for enhanced mineral prospectivity mapping, with reference to the orogenic gold mineralisation potential of the Kalgoorlie Terrane, Western Australia. *Aust. J. Earth Sci.* **2000**, *47*, 929–941. [CrossRef]
3. Partington, G.A. Exploration targeting using GIS: More than a digital light table. In Proceedings of the Geo Computing Conference, Brisbane, Australia, 29 September–1 October 2010; Volume 51, pp. 83–89.
4. Chung, C.F.; Agterberg, F.P. Regression models for estimating mineral resources from geological map data. *J. Int. Assoc. Math. Geol.* **1980**, *12*, 473–488. [CrossRef]
5. Crowe, W.A.; Nash, C.R.; Harris, L.B.; Leeming, P.M.; Rankin, L.R. The geology of the Rengali Province: Implications for the tectonic development of northern Orissa, India. *J. Asian Earth Sci.* **2003**, *21*, 697–710. [CrossRef]
6. Misra, S.; Gupta, S. Superposed deformation and inherited structures in an ancient dilational step-over zone: Post-mortem of the Rengali Province, India. *J. Struct. Geol.* **2014**, *59*, 1–17. [CrossRef]
7. Banerji, A. Ore genesis and its relationship to volcanism, tectonism, granitic activity, and metasomatism along the Singhbhum shear zone, eastern India. *Econ. Geol.* **1981**, *76*, 905–912. [CrossRef]
8. Ghosh, G.; Bose, S.; Das, K.; Dasgupta, A.; Yamamoto, T.; Hayasaka, Y.; Chakrabarti, K.; Mukhopadhyay, J. Transpression and juxtaposition of middle crust over upper crust forming a crustal scale flower structure: Insight from structural, fabric, and kinematic studies from the Rengali Province, eastern India. *J. Struct. Geol.* **2016**, *83*, 156–179. [CrossRef]

9. Nash, C.; Rankin, L.; Leeming, P.; Harris, L. Delineation of lithostructural domains in northern Orissa (India) from Landsat Thematic Mapper imagery. *Tectonophysics* **1996**, *260*, 245–257. [CrossRef]
10. Biswal, T.K.; De Waele, B.; Ahuja, H. Timing and dynamics of the juxtaposition of the Eastern Ghats Mobile Belt against the Bhandara Craton, India: A structural and zircon U-Pb SHRIMP study of the fold-thrust belt and associated nepheline syenite plutons. *Tectonics* **2007**, *26*, 1–21. [CrossRef]
11. Ghosh, G.; Bose, S.; Guha, S.; Mukhopadhyay, J.; Aich, S. Remobilization of the southern margin of the Singhbhum Craton, eastern India during the Eastern Ghats orogeny. *Indian J. Geol.* **2010**, *80*, 97–114.
12. Mahapatro, S.; Pant, N.; Bhowmik, S.; Tripathy, A.; Nanda, J. Archaean granulite facies metamorphism at the Singhbhum Craton–Eastern Ghats Mobile Belt interface: Implication for the Ur supercontinent assembly. *Geol. J.* **2012**, *47*, 312–333. [CrossRef]
13. Carranza, E.J.M.; Hale, M. Geologically Constrained Probabilistic Mapping of Gold Potential, Baguio District, Philippines. *Nat. Resour. Res.* **2000**, *9*, 237–253. [CrossRef]
14. An, P.; Moon, W.M.; Rencz, A.N. Application of fuzzy set theory to integrated mineral exploration. *Can. J. Explor. Geophys.* **1991**, *27*, 1–11.
15. Eddy, B.G.; Bonham-Carter, G.F.; Jefferson, C.W. Mineral resource assessment of the Parry Islands, high Arctic, Canada: A GIS-base fuzzy logic model. In Proceedings of the Canadian Conference on GIS, Ottawa, ON, Canada, 4–10 June 1995.
16. An, P.; Moon, W.M. An evidential reasoning structure for integrating geophysical, geological and remote sensing data. In Proceedings of the International Geoscience and Remote Sensing Symposium (IGARSS), Tokyo, Japan, 18–21 August 1993; pp. 1359–1361.
17. Carranza, E.J.M. From Predictive Mapping of Mineral Prospectivity to Quantitative Estimation of Number of Undiscovered Prospects. *Resour. Geol.* **2011**, *61*, 30–51. [CrossRef]
18. Carranza, E.J.M.; Hale, M. Evidential belief functions for data driven geologically constrained mapping of gold potential, Baguio district, Philippines. *Ore Geol. Rev.* **2002**, *22*, 117–132. [CrossRef]
19. Carranza, E.J.M.; Woldai, T.; Chikambwe, E.M. Application of data driven evidential belief functions to prospectivity mapping for aquamarine-bearing pegmatites, Lundazi District, Zambia. *Nat. Resour. Res.* **2005**, *14*, 47–63. [CrossRef]
20. Carranza, E.J.M.; Sadeghi, M. Predictive mapping of prospectivity and quantitative estimation of undiscovered VMS deposits in Skellefte district (Sweden). *Ore Geol. Rev.* **2010**, *38*, 219–241. [CrossRef]
21. Carranza, E.J.M. *Geochemical Anomaly and Mineral Prospectivity Mapping in GIS. Handbook of Exploration and Environmental Geochemistry*; Elsevier: Amsterdam, The Netherlands, 2009; Volume 11.
22. Bonham-Carter, G.F.; Agterberg, F.P.; Wright, D.F. Weights of evidence modeling: A new approach to mapping mineral potential. In *Statistical Applications in the Earth Sciences*; Agterberg, F.P., Bonham-Carter, G.F., Eds.; Geological Survey of Canada; Canadian Government Publishing Centre: Ottawa, ON, Canada, 1989; pp. 171–183.
23. Carranza, E.J.M. Weights of evidence modeling of mineral potential: A case study using small number of prospects, Abra, Philippines. *Nat. Resour. Res.* **2004**, *13*, 173–187. [CrossRef]
24. Austin, J.R.; Blenkinsop, T.G. Local to regional scale structural controls on mineralisation and the importance of a major lineament in the eastern Mount Isa In lier, Australia: Review and analysis with autocorrelation and weights of evidence. *Ore Geol. Rev.* **2009**, *35*, 298–316. [CrossRef]
25. Arianne, F.; Craig, J.R.H. Mineral potential mapping in frontier regions: A Mongolian case study. *Ore Geol. Rev.* **2013**, *51*, 15–26.
26. Oh, H.J.; Lee, S. Regional Probabilistic and Statistical Mineral Potential, Mapping of Gold-Silver Deposits Using GIS in the Gangreung Area, Korea. *Resour. Geol.* **2008**, *58*, 171–187. [CrossRef]
27. Ernowo; Oktaviani, P. Regional probabilistic of gold-silver potential mapping using likelihood ratio models in Flores Island. In Proceedings of the 39th IAGI Annual Convention and Exhibition, Lombok, Indonesia, 22–25 November 2010.
28. Carranza, E.J.M.; Hale, M.; Faassen, C. Selection of coherent deposit-type locations and their application in data-driven mineral prospectivity mapping. *Ore Geol. Rev.* **2008**, *33*, 536–558. [CrossRef]
29. Singer, D.A.; Kouda, R. Application of a feed forward neural network in the search for Kuroko deposits in the Hokuroku District, Japan. *Mathmatical Geol.* **1996**, *28*, 1017–1023. [CrossRef]
30. Oh, H.J.; Lee, S. Application of Artificial Neural Network for GoldSilver Deposits Potential Mapping: A Case Study of Korea. *Nat. Resour. Res.* **2011**, *19*, 103–124. [CrossRef]
31. Surip, N.; Hamzah, A.H.; Zakaria, M.R.; Napiah, A.; Talib, J.A. Mapping of gold in densely vegetated area using remote sensing and GIS techniques in Pahang, Malaysia. In Proceeding of Asian Conference on Remote Sensing (ACRS), Kuala Lumpur, Malaysia, 12–16 November 2007.
32. McMillan, M.; Haber, E.; Peters, B.; Fohring, J. Mineral prospectivity mapping using a VNet convolutional neural network. *Lead. Edge* **2021**, *40*, 99–105. [CrossRef]
33. Xu, Y.; Li, Z.; Xie, Z.; Cai, H.; Niu, P.; Liu, H. Mineral prospectivity mapping by deep learning method in Yawan-Daqiao area, Gansu. *Ore Geol. Rev.* **2021**, *138*, 104316. [CrossRef]
34. Ghosh, S.P.; Behere, S.N.; Mohanty, G. *Report on the Exploration for Basemetals In the Extension Area of Adash Copper Prospect, Sambalpur District, Orissa*; GSI Unpublished Report; Geological Survey of India: Kolkata, India, 1993.
35. Ghosh Roy, A.K. *Petrological Studies of The Mafic-Ultramafic Rocks Occurring Along the Contact Pegion Of Eastern Ghat Belt and Iron Ore Group in Parts of Sambalpur and Deogarh Districts, Orissa*; Unpublished Interim Progress Report of Geological Survey of India; Geological Survey of India: Kolkata, India, 1998.

36. Rana, G.; Rout, S.P.; Roychowdhury, K. *Preliminary Investigation for Ree In the Contact Zone Between Eastern Ghats Mobile Belt and Singhbhum Craton Around Kankarkhol in Parts of Deogarh District, Odisha (UNFC Stage-G4)*; Unpublished Report of Geological Survey of India; Geological Survey of India: Kolkata, India, 2017.
37. Rao, S.A.; Saha, T.K. *Systematic Geological Mapping in Deogarh Sub- Division, Sambalpur Dist, Orissa*; Unpublished Progress Report of Geological Survey of India; Geological Survey of India: Kolkata, India, 1972.
38. Naskar, D.C.; Mukherjee, R.; Singh, A.K.; Kumar, A. Systematic geophysical mapping in parts of Angul, Sambalpur, Sundargarh and Deogarh districts of Odisha, to delineate subsurface structure. *Richa Raghav Singh Prabodh Kumar Kushwaha SP Maurya Rohtash Kumar* **2021**, *25*, 32–47.
39. Talukdar, D.; Raul, A.K.; Gouda, H.C. *Integration of Geological, Geochemical and Geophysical Data in Parts of Adash Area, Odisha with Limited Field-Check for the Search of Potential Mineral Blocks*; Unpublished Report of Geological Survey of India; Geological Survey of India: Kolkata, India, 2019.
40. Arrieta, A.B.; Díaz-Rodríguez, N.; Del Ser, J.; Bennetot, A.; Tabik, S.; Barbado, A.; García, S.; Gil-López, S.; Molina, D.; Benjamins, R. Explainable Artificial Intelligence (XAI): Concepts, taxonomies, opportunities and challenges toward responsible AI. *Inf. Fusion* **2020**, *58*, 82–115. [CrossRef]
41. Dikshit, A.; Pradhan, B. Interpretable and explainable AI (XAI) model for spatial drought prediction. *Sci. Total Environ.* **2021**, *801*, 149797. [CrossRef]
42. Behera, S.; Panigrahi, M.K.; Pradhan, A. Identification of geochemical anomaly and gold potential mapping in the Sonakhan Greenstone belt, Central India: An integrated concentration-area fractal and fuzzy AHP approach. *Appl. Geochem.* **2019**, *107*, 45–57. [CrossRef]
43. Zhang, N.; Zhou, K.; Li, D. Back-propagation neural network and support vector machines for gold mineral prospectivity mapping in the Hatu region, Xinjiang, China. *Earth Sci. Inform.* **2018**, *11*, 553–566. [CrossRef]
44. Raines, G.L. Evaluation of weights of evidence to predict epithermal-gold deposits in the Great Basin of the Western United States. *Nat. Resour. Res.* **1999**, *8*, 257–276. [CrossRef]
45. Bonham-Carter, G.F.; Agterberg, F.P.; Wright, D.F. Integration of geological datasets for gold exploration in Nova Scotia. *Photogramm. Eng. Remote Sens.* **1998**, *54*, 1585–1592.
46. Dasgupta, A.; Bose, S.; Das, K.; Ghosh, G. Petrological and geochemical evolution of the Central Gneissic Belt, Rengali Province, eastern India: Implications for the Neoarchean growth and orogenesis. *J. Asian Earth Sci.* **2017**, *146*, 1–19. [CrossRef]
47. Ghosh, G.; Bose, S. Deformation and metamorphic history of the Singhbhum Craton vis–à–vis peripheral mobile belts, eastern India: Implications on Precambrian crustal processes. *J. Mineral. Petrol. Sci.* **2020**, *115*, 70–87. [CrossRef]
48. Saha, A.K. Crustal Evolution of Singhbhum North Orissa Eastern India. In *Memorendum of Geological Society of India*; Geological Survey of India: Kolkata, India, 1994.
49. Panda, P.K.; Patra, P.C.; Nanda, J.K. Petrochemistry of the alkaline rocks of Rairakhol–Kankarakhol belt, Sambalpur and Deogarh districts, Orissa. *Geol. Surv. India Spec. Publ.* **1998**, *44*, 307–314.
50. Panda, P.K.; Patra, P.C.; Patra, R.N.; Nanda, J.K. Nepheline syenite from Rairakhol, Sambalpur district, Orissa. *J. Geol. Soc. India* **1993**, *41*, 144–151.
51. Ranjan, S.; Upadhyay, D.; Abhinay, K.; Pruseth, K.L.; Nanda, J.K. Zircon geochronology of deformed alkaline rocks along the Eastern Ghats Belt margin: India–Antarctica connection and the Enderbia continent. *Precambrian Res.* **2018**, *310*, 407–424. [CrossRef]
52. Sheikh, J.M.; Patel, S.C.; Champati, A.K.; Madhavan, K.; Behera, D.; Naik, A.; Gerdes, A. Nepheline syenite intrusions from the Rengali Province, eastern India: Integrating geological setting, microstructures, and geochronological observations on their syntectonic emplacement. *Precambrian Res.* **2020**, *346*, 105802. [CrossRef]
53. Ganguly, P.K.; De, S.K.; Chattopadhyay, R.C. *Report on the test geophysical investigations for sulphide mineralisation near Medinipur-Budido villages, Sambalpur district, Orissa*; (unpublished progress report for the F.S. 1974–1975); Geological Survey of India: Kolkata, India, 1975.
54. Karim, M.A.; Hussain, A.; Mohanty, S.N. *Interim Report on The Regional Geochemical Survey in Deogarh Greenstone Belt for Assessing Economic Mineral Potential*; unpublished interim report; Geological Survey of India: Kolkata, India, 2011.
55. Ahmadirouhani R, Karimpour M-H, Rahimi B, Malekzadeh-Shafaroudi A, Pour AB, Pradhan B Integration of SPOT-5 and ASTER satellite data for structural tracing and hydrothermal alteration mineral mapping: Implications for Cu–Au prospecting. *Int. J. Image Data Fusion* **2018**, *9*, 237–262. [CrossRef]
56. Bhukosh Portal, Geological Survey of India. Available online: https://bhukosh.gsi.gov.in/Bhukosh/Public (accessed on 10 July 2021).
57. Sun, T.; Chen, F.; Zhong, L.; Liu, W.; Wang, Y. GIS-based mineral prospectivity mapping using machine learning methods: A case study from Tongling ore district, eastern China. *Ore Geol. Rev.* **2019**, *109*, 26–49. [CrossRef]
58. Sheikhrahimi, A.; Pour, A.B.; Pradhan, B.; Zoheir, B. Mapping hydrothermal alteration zones and lineaments associated with orogenic gold mineralization using ASTER data: A case study from the Sanandaj-Sirjan Zone, Iran. *Adv. Space Res.* **2019**, *63*, 3315–3332. [CrossRef]
59. Wang, G.; Pang, Z.; Boisvert, J.B.; Hao, Y.; Cao, Y.; Qu, J. Quantitative assessment of mineral resources by combining geostatistics and fractal methods in the Tongshan porphyry Cu deposit (China). *J. Geochem. Explor.* **2013**, *134*, 85–98. [CrossRef]

60. Kashani, S.B.M.; Abedi, M.; Norouzi, G.-H. Fuzzy logic mineral potential mapping for copper exploration using multi-disciplinary geo-datasets, a case study in seridune deposit, Iran. *Earth Sci. Inform.* **2016**, *9*, 167–181. [CrossRef]
61. Motta, J.G.; Faria, I.R. A mineral potential mapping approach for supergene nickel deposits in southwestern São Francisco Craton, Brazil. *Braz. J. Geol.* **2016**, *46*, 261–273. [CrossRef]
62. Chung, C.-J.; Keating, P.B. Mineral potential evaluation based on airborne geophysical data. *Explor. Geophys.* **2002**, *33*, 28–34. [CrossRef]
63. Porwal, A.; Carranza, E.; Hale, M. Knowledge-driven and data-driven fuzzy models for predictive mineral potential mapping. *Nat. Resour. Res.* **2003**, *12*, 1–25. [CrossRef]
64. Dentith, M.; Mudge, S.T. *Geophysics for the Mineral Exploration Geoscientist*; Cambridge University Press: Cambridge, UK, 2014.
65. Moreira, C.A.; Ilha, L.M. Prospecção geofísica em ocorrência de cobre localizada na bacia sedimentar do Camaquã (RS). *Rem Rev. Esc. De Minas* **2011**, *64*, 305–311. [CrossRef]
66. Doyle, H. Geophysical exploration for gold? A review. *Explor. Geophys.* **1986**, *17*, 169–180. [CrossRef]
67. Foster, B. *Gold Metallogeny and Exploration*; Springer: Dordrecht, The Netherlands, 1993; 432p.
68. Bolouki, S.M.; Ramazi, H.R.; Maghsoudi, A.; Beiranvand Pour, A.; Sohrabi, G. A remote sensing-based application of bayesian networks for epithermal gold potential mapping in Ahar-Arasbaran area, NW Iran. *Remote Sens.* **2020**, *12*, 105. [CrossRef]
69. Van der Meer, F.D.; Van der Werff, H.M.; Van Ruitenbeek, F.J.; Hecker, C.A.; Bakker, W.H.; Noomen, M.F.; Van Der Meijde, M.; Carranza, E.J.M.; De Smeth, J.B.; Woldai, T. Multi-and hyperspectral geologic remote sensing: A review. *Int. J. Appl. Earth Obs. Geoinf.* **2012**, *14*, 112–128. [CrossRef]
70. LeCun, Y.; Bottou, L.; Bengio, Y.; Haffner, P. Gradient-based learning applied to document recognition. *Proc. IEEE* **1998**, *86*, 2278–2324. [CrossRef]
71. Krizhevsky, A.; Sutskever, I.; Hinton, G.E. Imagenet classification with deep convolutional neural networks. *Adv. Neural Inf. Processing Syst.* **2012**, *25*, 1097–1105. [CrossRef]
72. Kingma, D.P.; Ba, J. Adam: A method for stochastic optimization. *arXiv* **2014**, arXiv:1412.6980.
73. Lundberg, S.M.; Lee, S.-I. A unified approach to interpreting model predictions. In Proceedings of the 31st International Conference on Neural Information Processing Systems, Long Beach, CA, USA, 4–9 December 2017; pp. 4768–4777.
74. Mitchell, A. *TM Machine Learning in Ecosystem Informatics and Sustainability*; McGraw-Hill Science/Engineering/Math: New York, NY, USA, 1997.
75. Severyn, A.; Moschitti, A. Unitn: Training deep convolutional neural network for twitter sentiment classification. In Proceedings of the 9th International Workshop on Semantic Evaluation (SemEval 2015), Denver, CA, USA, 4–5 June 2015; pp. 464–469.
76. Zhao, S.; Guo, Y.; Sheng, Q.; Shyr, Y. Advanced heat map and clustering analysis using heatmap3. *BioMed Res. Int.* **2014**, *2014*, 986048. [CrossRef] [PubMed]
77. Chakravarti, R.; Singh, S.; Venkatesh, A.; Patel, K.; Sahoo, P. A modified placer origin for refractory gold mineralization within the Archean radioactive quartz-pebble conglomerates from the eastern part of the Singhbhum Craton, India. *Econ. Geol.* **2018**, *113*, 579–596. [CrossRef]
78. Singh, S.; Chakravarti, R.; Barla, A.; Behera, R.C.; Neogi, S. A holistic approach on the gold metallogeny of the Singhbhum crustal province: Implications from tectono-metamorphic events during the Archean-Proterozoic regime. *Precambrian Res.* **2021**, *365*, 106376. [CrossRef]
79. Macdonald, E. *Handbook of Gold Exploration and Evaluation*; Elsevier: Amsterdam, The Netherlands, 2007.
80. Goldfarb, R.J.; Groves, D.I.; Gardoll, S. Orogenic gold and geologic time: A global synthesis. *Ore Geol. Rev.* **2001**, *18*, 1–75. [CrossRef]
81. Goldfarb, R.; Baker, T.; Dubé, B.; Groves, D.I.; Hart, C.J.; Gosselin, P. *Distribution, Character and Genesis of Gold Deposits in Metamorphic Terranes*; Society of Economic Geologists: Littleton, CO, USA, 2005.
82. Goldfarb, R.J.; Groves, D.I. Orogenic gold: Common or evolving fluid and metal sources through time. *Lithos* **2015**, *233*, 2–26. [CrossRef]
83. Biswas, S. Geological Setup for Gold Prospects and Deposits in India. *Conf. GSI* **2021**, 1–13. [CrossRef]
84. Sui, J. Geochronology and Genesis of the Zaozigou Gold Deposit, Gansu Province, China. Ph.D. Thesis, China University of Geosciences, Wuhan, China, 2012. (In Chinese with English Abstract)
85. Zhang, S.; Carranza, E.J.M.; Wei, H.; Xiao, K.; Yang, F.; Xiang, J.; Zhang, S.; Xu, Y. Data-driven mineral prospectivity mapping by joint application of unsupervised convolutional auto-encoder network and supervised convolutional neural network. *Nat. Resour. Res.* **2021**, *30*, 1011–1031. [CrossRef]